

UNSCAR: Universal, Scalable, Controllable, and Adaptable Image Restoration

Debabrata Mandal¹ Soumitri Chattopadhyay² Yujie Wang¹
 Marc Niethammer² Praneeth Chakravarthula¹

¹ University of North Carolina at Chapel Hill

² University of California, San Diego

Abstract. Universal image restoration aims to recover clean images from arbitrary real-world degradations using a single inference model. Despite significant progress, existing all-in-one restoration networks do not scale to multiple degradations. As the number of degradations increases, training becomes unstable, models grow excessively large, and performance drops across both seen and unseen domains. In this work, we show that scaling universal restoration is fundamentally limited by interference across degradations during joint learning, leading to *catastrophic task forgetting*. To address this challenge, we introduce a unified inference pipeline with a multi-branch mixture-of-experts architecture that decomposes restoration knowledge across specialized task-adaptable experts. Our approach enables *scalable* learning (over sixteen degradations), *adapts and generalizes* robustly to unseen domains, and supports *user-controllable restoration* across degradations. Beyond achieving superior performance across benchmarks, this work establishes a new design paradigm for scalable and controllable universal image restoration.

arXiv:2603.07406v1 [cs.CV] 8 Mar 2026

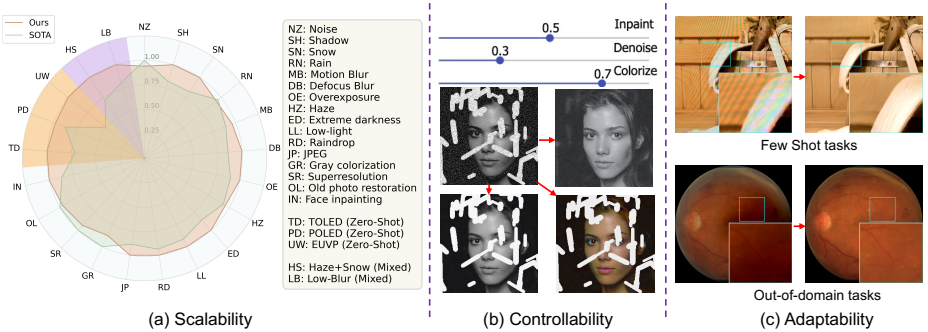


Fig. 1: We introduce UNSCAR, a universal image restoration model that can handle $2\times$ more degradations than previously explored, achieving state-of-the-art performance across multiple benchmarks. Our framework also enables user-controllable restoration via degradation-control sliders and supports few-shot adaptation (down to one-shot) with strong out-of-distribution generalization on challenging medical imaging datasets.

1 Introduction

Image restoration has progressed from heuristic pixel-level algorithms to powerful black-box deep neural network models [12, 19, 21, 26, 31, 45, 49–51, 59, 62, 63,

Table 1: Comparison with prior image restoration works. Factors are denoted as fully met ✓, partially met (✓), or unmet ✗.

Method	Venue	Unified Model	Mixed Restoration	Automatic	Scalability	Adaptability	Control Modality	#Primary Tasks
Restormer [80]	CVPR'22	✗	✗	✗	✗	(✓)	—	1
AutoDIR [31]	ECCV'24	(✓)	(✓)	(✓)	✗	✗	—	4
DA-CLIP [50]	ICLR'24	✗	✗	✓	✗	✗	—	10
OneRestore [26]	ECCV'24	✓	✓	(✓)	(✓)	✗	Limited	3
MPerceiver [5]	CVPR'24	✓	✓	✓	✓	(✓)	—	8
CAPTNet [24]	TCVST'24	✓	✗	✗	✗	✗	—	4
RestoreVAR [62]	ICLR'26	✓	✓	(✓)	✗	✗	—	4
Defusion [49]	CVPR'25	✓	(✓)	✓	✓	✗	—	8
UniRes [93]	ICCV'25	✓	✓	✓	(✓)	(✓)	—	4
UARE [44]	arXiv'25	✓	✓	✓	✗	(✓)	Text	5
FluxIR [17]	CVPR'25	✓	✗	(✓)	(✓)	✗	Text	2
UniCoRN [51]	WACV'26	✓	✓	(✓)	✓	(✓)	Text	6
UNSCAR (Ours)	—	✓	✓	✓	✓	✓	Sliders	16

[69, 80]. Recent approaches demonstrate that a single architecture can address multiple restoration tasks, simplifying model design, storage, and deployment across different ill-posed imaging problems [12, 21, 59, 80]. However, these unified architectures typically require *separate training for each degradation type* [59, 80]. As a result, they struggle with mixed or unseen degradations, where models must first identify degradation before performing restoration [31, 50].

Recent universal or all-in-one restoration (AIR) methods attempt to address this challenge by jointly learning multiple degradations within a single framework. This allows for restoration under mixed or unknown conditions [5, 50, 51, 62, 63]. However, AIR models trained across multiple degradation removal tasks often suffer from catastrophic forgetting [35, 75]. This leads to a performance drop as the number and diversity of degradation types increase. Furthermore, generative restoration models trained on natural scenes often fail on out-of-distribution data, such as surgical [76], medical [67], or satellite imagery [6]. When guided by standard control modalities (e.g., text prompts) [5, 17, 44], these models frequently struggle due to limited domain-specific training data. As a result, current AIR approaches remain *restricted* to training data domains and lack mechanisms for *forgetting-free adaptation*. Additionally, most existing AIR methods focus on blind restoration, providing limited control over the image recovery process.

In this work, we address these challenges by introducing **UNSCAR**, a scalable and controllable universal image restoration framework capable of handling multiple degradations (more than 16 demonstrated), significantly extending the scope of prior approaches [5, 50, 51] (see Tab. 1). Our method builds upon the UniCoRN architecture [51], which introduced low-level visual cues and mixture-of-experts (MoE) adapters for generative restoration. We extend this design with several architectural improvements aimed at improving scalability and robustness: *(i)* unified encoding of richer low-level visual priors, *(ii)* task-aware degradation-content disentangled embeddings, *(iii)* bi-directional feedback between control and generative branches, and *(iv)* novel residual-attention MoE blocks that reduce cross-task interference. Extensive experiments across single, synthetically mixed, and complex degradation benchmarks demonstrate the robustness, scalability and universality of the proposed UNSCAR architecture.

Beyond scalability, we introduce *fine-grained controllability* into the restoration process. Inspired by controllable generative models [36, 54, 65] and concept editing methods [22, 23], we propose *(v)* a degradation control slider mechanism that

allows users to modify restoration behavior. As illustrated in Fig. 1, the slider softly reweights expert activations, overriding the default MoE-based restoration strategy to enable interpretable and flexible degradation manipulation. Finally, we demonstrate that UNSCAR can *adapt efficiently to unseen restoration* tasks. Using *(vi)* a lightweight parameter-efficient fine-tuning (PEFT) approach, our model can be adapted to new restoration tasks in *zero-shot* or *few-shot* settings (~ 1 –50 samples). Our experiments on out-of-distribution medical imaging tasks, including laparoscopic image de-smoking [76] and fundus image restoration [67], demonstrate robust generalization and efficient adaptation.

As summarized in Tab. 1, UNSCAR constitutes a paradigm shift for scalable and controllable universal image restoration, demonstrating improved flexibility for practical image restoration applications.

2 Related works

Single-degradation Image Restoration: Early deep-learning approaches for image restoration focused on addressing a *single known degradation*, such as haze, smoke, noise, low-light, or low-contrast. Representative task-specific models include those for dehazing [19, 39, 69], denoising [20, 37], and deblurring [13, 83]. Another line of work proposed unified architectures that can be trained separately for different restoration tasks [21, 40, 47, 73, 73, 80]. These enable end-to-end mapping from degraded images to clean outputs, and remain largely task-agnostic. However, they suffer from two fundamental limitations: (i) limited scalability to diverse real-world degradations [51], and (ii) limited availability, or unavailability, of high-quality degradation-specific training data in practice. Overcoming these limitations, we propose a *unified, degradation-agnostic, scalable and adaptable universal image restoration model* for practical real-world scenarios.

Multi-degradation Image Restoration: Recent work has focused on simultaneously modeling multiple degradations to reflect real-world images which typically contain several co-existing corruptions [31, 41, 44, 50, 51, 93]. These approaches include degradation-specific modules [9, 70] or embeddings [41, 59], neural architecture search [43], and degradation-aware prompt-based conditioning [46, 59]. While these methods show improved robustness, they remain limited in scalability and adaptability to diverse degradations [44, 51, 62], restricting their practical use – challenges which we address in this work.

Conditional Diffusion Models and Controllable Generation: Diffusion models [29, 34, 65, 85] have recently emerged as the de facto paradigm for controllable visual generation across images [65], videos [7], medical scans [89], and 3D objects [58]. Popular frameworks include Stable Diffusion [65], ControlNet [85], DreamBooth [66], Flux [36], and Wan [71]. Conditional diffusion models allow users to control the generation process through signals such as text prompts [65], structural guidance (e.g., edge, depth, color maps) [85, 91], or via personalization [66]. Extensions to the ControlNet architecture [86] have further enhanced controllability, such as ControlNet++ [42] which uses consistency rewards, ControlNet-XS [81] which provides early feedback injection, UniControlNet [90] for fusing control information, and ControlNeXt [57] for efficient fine-tuning. More recently, low-rank adapters have enabled fine-grained editing

in generative models [22, 23]. Inspired by these advances, our work introduces mechanisms for *adaptability* and *precise control* for real-world image restoration.

Universal Image Restoration via Generative Models: Recent research has explored universal image restoration using conditional diffusion models [28, 45, 50, 92], where the conditioning signal encodes degradation-relevant information. For example, DA-CLIP [50] and D4IR [72] train degradation-aware encoders using contrastive learning [60] to guide diffusion-based restoration. AutoDIR [31] identifies the dominant degradation before applying a structure-corrected diffusion model for restoration. MPerceiver [5] combines prompt learning and cross-modal feature inversion for stronger visio-linguistic synergy for text-conditioned restoration. More recent works further extend this paradigm. UniCoRN [51] employs low-level visual estimates with ControlNet-style conditioning [85] and MoE modules, RestoreVAR [62] uses visual auto-regressive restoration, UniRes [93] generates multiple text-driven restorations and combines them at inference time, and UARE [44] aligns image quality assessment and restoration learning through interleaved data and a progressive schedule for learning single to multiple degradations. UNSCAR follows this conditional generative restoration paradigm while introducing several architectural innovations for improving scalability and adaptability across diverse degradation settings.

3 Methodology

3.1 Preliminaries: Unified Controllable Restoration

Given a degraded image \tilde{I} , an image restoration process typically involves: (1) identifying present degradations, (2) balancing their restoration strengths, and (3) predicting a residual restoration direction R such that $I^* = \tilde{I} + R$. UNICORN [51] realizes this paradigm in a latent diffusion framework through conditioning mechanisms and control pathways for generative restoration. It extracts task-specific low-level visual cues (e.g., edge, haze, noise maps) to identify degradations, uses lightweight MoE adapters to weight restoration strengths across the identified degradation types, and injects the balanced control signals into the latent space denoiser via a ControlNet-style mechanism.

Limitations of UniCoRN. While effective, this design faces scalability challenges: (1) Degradation-specific cue selection requires manually defined mappings, which become prohibitive as the number of degradations grows. (2) Maintaining separate control generation pathways per degradation through ControlNet introduces significant parameter overhead and limits scalability. (3) UniCoRN employs ultra-lightweight MoE adapters to generate spatially varying weights that balance restoration signals across degradation types, and adopts curriculum learning for mixed degradations. However, as degradation types increase, expert routing becomes increasingly difficult to interpret and control, particularly under limited mixed-degradation training data. These limitations motivate our redesigned architecture for scalable and user-controllable restoration.

3.2 UNSCAR

UNSCAR is designed to scale universal restoration along two axes: representation scaling and conditional capacity scaling. At the representation level, we en-

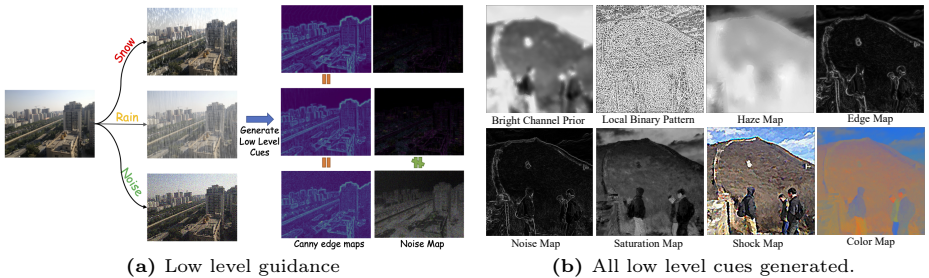


Fig. 2: Low-level cues. (a) Low-level cues provide discriminative signals across degradation types, enabling automatic restoration. (b) Our framework leverages diverse cues such as edges, color statistics, noise, and transmission, to characterize the input scene.

hance degradation observability and discriminability while removing manual task-specific routing. At the architectural level, we redesign the conditional control pathway to scale to diverse degradations without proportional growth in parameters or computation. Finally, we introduce lightweight practical extensions to improve restoration fidelity, controllability, and adaptability to new tasks.

1) Unified and Degradation-Aware Guidance Representation. As degradation diversity increases, reliable distinction among heterogeneous and mixed degradations becomes critical. As discussed in Sec. 3.1, manual task-to-cue specification limits scalability when the degradation space expands. To resolve this, we replace task-specific cue pathways with a unified guidance encoder.

Richer Low-Level Structural Priors. To improve degradation observability, as shown in Fig. 2, we expand the pool of low-level visual cues extracted from the degraded image \tilde{I} , approximately doubling the number used in UniCoRN. These cues provide complementary structural signals across degradation types (e.g., noise amplification, haze patterns, color shifts), enhancing the model’s ability to identify degradation characteristics.

Unified Guidance Encoding. Instead of maintaining task-specific cue pathways, we adopt a unified guidance encoder that jointly processes the degraded image and all extracted cues. Each input (the degraded image \tilde{I} and the enriched low-level cues $\{v_i\}$) is encoded independently through a lightweight chain of n Nonlinear Activation Free (*NAF*) layers [12]. The resulting features are aggregated via summation before being passed to the diffusion backbone (see Fig. 3):

$$\mathbf{g} = \text{NAF}_0^n(\tilde{I}) + \sum_i \text{NAF}_i^n(v_i), \quad (1)$$

where \mathbf{g} denotes the unified guidance representation shared across all degradation tasks. Here, v_i represents the enriched low-level cues, and i indexes the corresponding *NAF* encoding branches. This unified encoding eliminates manual cue-to-task specification and enables the model to implicitly infer degradation composition from shared structural representations.

Degradation-Aware Embedding Augmentation. As degradation diversity increases, precise task differentiation within the conditional pathway becomes essential to prevent feature interference. Control signals from heterogeneous tasks may overlap (e.g., rain+fog vs. rain or fog), resulting in ambiguous conditional modulation and degraded restoration quality, particularly under mixed-

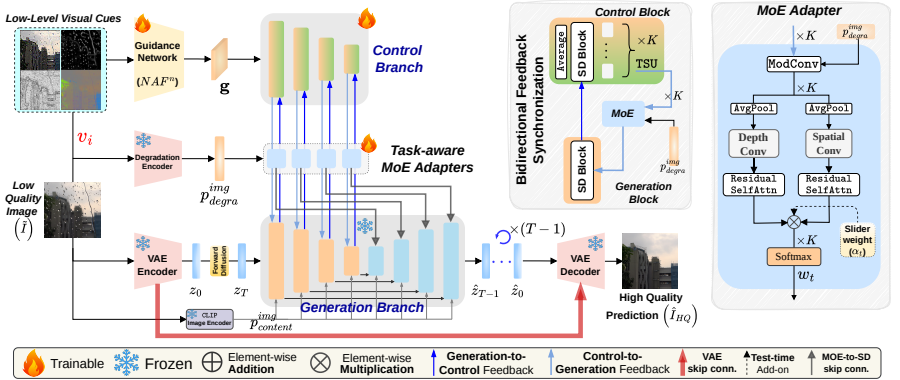


Fig. 3: UNSCAR architecture. We leverage low-level visual guidance within a bidirectional feedback, controllable generative network with mixture-of-experts. This enables unified image restoration across multiple simultaneous degradations.

degradation settings. To enhance task discriminability, we introduce degradation-aware embeddings built upon a visual-language model [50]. Specifically, we augment the CLIP image encoder [61] with an additional degradation controller head, which disentangles content embeddings $p_{content}^{img}$ from degradation embeddings p_{degra}^{img} (see Fig. 4). Together, these designs establish a unified and degradation-aware guidance representation that scales to diverse and mixed-degradations.

2) Capacity-Efficient ControlNet. To realize capacity-efficient conditioning, we enhance the conditional pathway through control signal compression, efficient mixture-of-experts adapters and bidirectional feedback synchronization (Fig. 3).

Shared Control Compression. As the number of degradation tasks increases, naively forwarding each task-specific control signal \mathcal{F}_t (t indexes the degradation tasks) independently through heavy ControlNet layers (L) results in redundant computation and quickly becomes a scalability bottleneck. To maintain capacity-efficient conditioning, we introduce a lightweight squeeze-and-excite mechanism that amortizes control computation across tasks. The *squeeze* operation aggregates task-specific control features \mathcal{F}_t via averaging and producing a shared control representation s^k . The *excitation* stage then redistributes this shared representation to each task through task-specific modulation units (TSU) [51],

$$s^k = \text{Average}(\mathcal{F}_t^{k-1}), \mathcal{F}_t^k = \text{TSU}_t(L^k(s^k)); \mathcal{F}_t^0 = \mathbf{g}. \quad (2)$$

L^k denotes k -th shared control layer. This design maintains task-specific modulation while avoiding repeated control computations, enabling improved effective conditional capacity under limited parameter capacity and compute budgets.

Scaling the Mixture-of-Experts Adapter. Many prior all-in-one restoration methods rely on inference-time weighting to balance restoration trajectories [51, 93]. In contrast, we integrate task balancing directly within the mixture-of-experts (MoE) routing mechanism. While UniCoRN employs multi-dimensional spatially-varying routing, such routing becomes increasingly complex and difficult to interpret as the number of degradation types grows. We instead adopt a global task-level routing strategy that predicts a single normalized weight vector over

degradation tasks. Specifically, we compress \mathcal{F}_t via spatial average pooling with factor $\downarrow f$, yielding a downsampled representation of size $(H \times W) \rightarrow (\frac{H}{f} \times \frac{W}{f})$, which is subsequently processed through depth-wise and spatial convolutions [51], followed by residual attention blocks [77]. The resulting features are projected to a task-level weight vector $\mathbf{w} \in \mathbb{R}^T$, normalized via softmax to enforce $\sum_t w_t^k = 1$. To further enhance degradation awareness, each expert router E^k is conditioned on the degradation embeddings p_{degra}^{img} via style modulation [33]:

$$\mathcal{F}_{\text{fused}}^k = \sum \underbrace{E^k((\mathcal{F}_t^k) \downarrow_f; p_{degra}^{img})}_{w_t^k} \cdot \mathcal{F}_t^k. \quad (3)$$

$\mathcal{F}_{\text{fused}}^k$ denotes the fused feature at layer k . This global routing improves conditional capacity while maintaining parameter and computational efficiency, enabling scalable multi-degradation restoration.

Bidirectional Feedback Synchronization. UniCoRN follows the original ControlNet paradigm, where feedback signals are injected only into the decoder layers of the diffusion backbone. The backbone encoder remains frozen and processes degraded inputs without intermediate correction. Under this decoder-only injection design, degradation-induced artifacts accumulate in encoder representations before any corrective modulation is applied. The decoder-side control branch must then compensate for these errors retroactively, increasing correction strain and limiting effective conditional capacity as degradation diversity grows. To alleviate this structural imbalance, we adopt a bidirectional synchronization mechanism, inspired by [81], that enables feature exchange between the control encoder to the frozen backbone encoder:

$$\mathcal{F}_{\text{fused}}^{k+1} = L_c^{k+1}(\mathcal{F}_{\text{fused}}^k + \mathcal{F}_b^k), \quad \mathcal{F}_b^{k+1} = L_b^{k+1}(\mathcal{F}_{\text{fused}}^k + \mathcal{F}_b^k), \quad (4)$$

where \mathcal{F}_b^k and \mathcal{F}_c^k denote backbone and control signal at layer k . This early feature exchange distributes correction across the network, increasing effective conditional capacity yet keeping a lightweight control branch ($\sim 0.2 \times$ less parameters).

3) Practical Extensions. Complementing the representation and control redesign that address scalability, we further introduce lightweight extensions to enhance fidelity and expand the practical usability of the framework.

Residual VAE Refinement. Due to the lossy nature of the variational autoencoder (VAE) used in SD 1.5 [65], we introduce a simple modification to the decoder architecture to better suit image restoration, where faithful reconstruction is required rather than hallucination. Specifically, we forward the intermediate activations of the degraded input image from the VAE encoder to the decoder after the diffusion-based correction is performed in our model. These encoder features are then alpha-blended with the decoder’s upsampled activations at each level using zero-initialized residual convolutional blocks.

Controllable Restoration via Sliders. Controlling the image restoration process enhances model customizability for photo editing applications and provides greater transparency into its working principles, in contrast to prior black-box all-in-one restoration methods. We introduce a controllability mechanism within our universal restoration framework by associating each restoration task (e.g.,

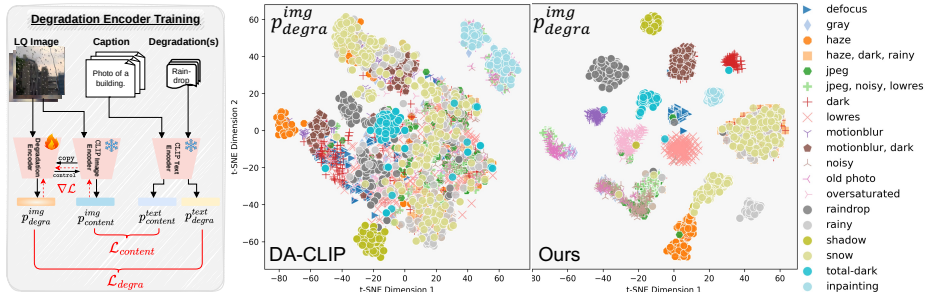


Fig. 4: Degradation-aware embeddings. Our degradation-aware training framework (left) learns an auxiliary degradation encoder cloned from the CLIP image encoder trained with SigLIP loss [82]. The resulting embeddings provide clear separation between single- and mixed-degradation tasks while maintaining proximity across related degradations.

deblurring, denoising, dehazing) with an independent user-controlled intensity slider. This design enables fine-grained control over different degradation types rather than relying on a single global restoration strength. Formally, let w_t denote the fusion control weight generated by the mixture-of-expert adapter for a specific degradation type ($t \in T$). For each degradation, the user also specifies an intensity coefficient $\alpha_t \in [0, 1]$. The controlled fusion weights at layer k are computed as $\tilde{w}_t^k = \frac{\alpha_t w_t^k}{\sum_T \alpha_t w_t^k}$, which ensures $\tilde{w}_t^k \in [0, 1]$ and $\sum_t \tilde{w}_t^k = 1$. This task-wise re-weighting preserves the scale and stability of the latent representation while allowing continuous and independent control over each degradation.

Few-shot unseen task Adaptation. While our model generalizes to unseen degradations in natural images, adapting to significantly different Out-of-domain (OOD) images (e.g., medical imaging) remains challenging. Leveraging the modular design of our architecture, we enable efficient OOD adaptation by introducing an auxiliary low-level encoder head (NAF chain) that processes degraded images alongside the unified low-level encoder described before. For each new OOD dataset, we also duplicate a task-specific unit (TSU) similar to few-shot task adaptation case and its associated squeeze-excitation modules at each encoder layer, leaving the core mixture-of-experts blocks untouched. This lightweight extension enables effective adaptation to challenging domains, such as medical imaging, without disrupting previously learned restoration capabilities or inducing catastrophic forgetting.

3.3 Training Objectives and Strategy

During training, we adopt a training objective that enforces reconstruction fidelity and condition embedding supervision, and a routing stabilization strategy that stabilizes expert specialization.

Training Objectives. The overall objective is defined as, $\mathcal{L}_{\text{total}} = \mathcal{L}_{\text{LDM}} + \lambda_{\text{pixel}} \mathcal{L}_{\text{pixel}}$, where \mathcal{L}_{LDM} is the latent diffusion training objective, following the DDIM formulation [68] with ϵ -parameterization:

$$\mathcal{L}_{\text{diff}} = \mathbb{E}_{t, \epsilon} [\|\epsilon - \epsilon_{\theta}(x_t, t)\|^2; \{\mathcal{F}_{\text{fused}}^k\}], \quad (5)$$

where $\epsilon \sim \mathcal{N}(0, 1)$ denotes Gaussian noise, x_t is the noisy latent at timestep t , $\{\mathcal{F}_{\text{fused}}^k\}$ is the set of control feature from all intermediate layers and $\epsilon_{\theta}(x_t, t)$

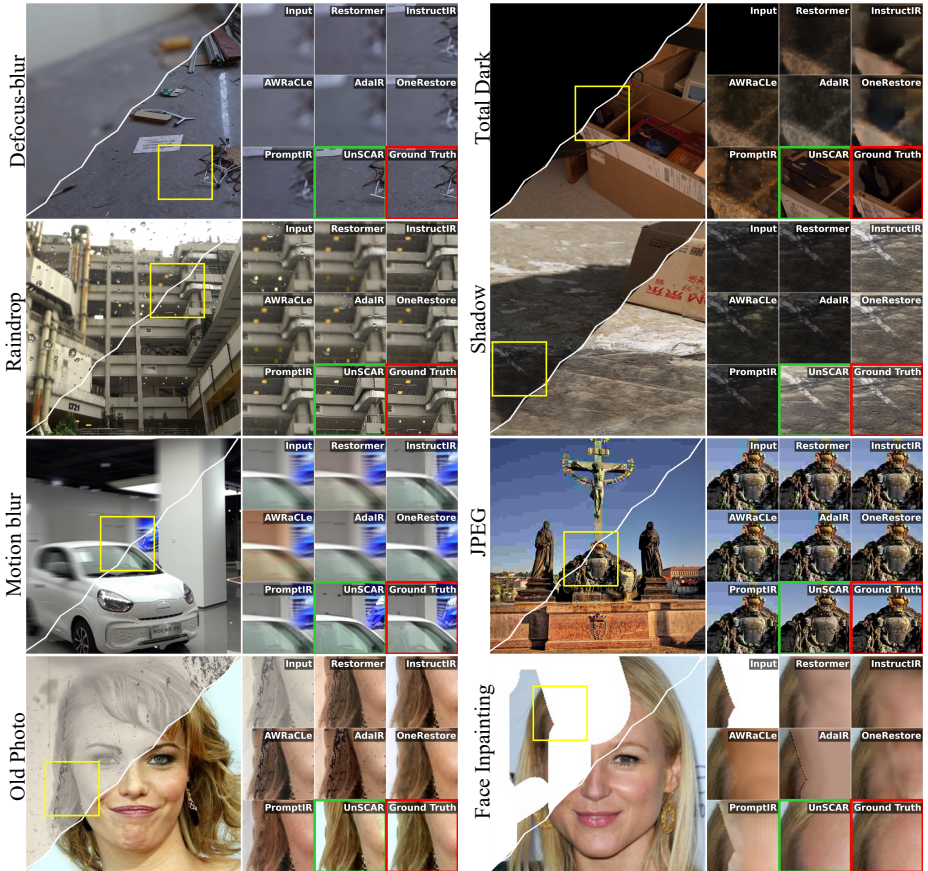


Fig. 5: Single-degradation restoration. UnSCAR produces sharper, higher-fidelity reconstructions across single-degradation tasks.

predicts the noise. $\mathcal{L}_{\text{pixel}}$ is a Pixel-Space Reconstruction Loss, which is introduced to mitigate hallucinated textures and structural artifacts. $\mathcal{L}_{\text{pixel}}$ is defined as:

$$\mathcal{L}_{\text{pixel}} = \gamma_1 \|x_{\text{gt}} - \mathcal{D}_\phi(\hat{z}_0)\|_1 + \gamma_2 \mathcal{L}_{\text{SSIM}}(x_{\text{gt}}, \mathcal{D}_\phi(\hat{z}_0)) + \gamma_3 \mathcal{L}_{\text{LPIPS}}(x_{\text{gt}}, \mathcal{D}_\phi(\hat{z}_0)), \quad (6)$$

where x_{gt} is the ground-truth image, \mathcal{D}_ϕ denotes the VAE decoder with encoder skip-connections, and \hat{z}_0 is the predicted clean latent from noise ($\epsilon(x_t, t)$) at time step t . λ_{pixel} and $\gamma_{1,2,3}$ are a balancing weights. $\lambda_{\text{pixel}} = \gamma_1 = \gamma_3 = 0.4$, $\gamma_2 = 0.2$.

Condition Embedding Supervision. To enable accurate degradation discrimination and task-aware routing, we supervise condition embeddings via

$$\mathcal{L}_{\text{cond}} = \mathcal{L}_{\text{content}}(p_{\text{content}}^{\text{img}}) + \mathcal{L}_{\text{degradation}}(p_{\text{degra}}^{\text{img}}). \quad (7)$$

$p_{\text{content}}^{\text{img}}$ and $p_{\text{degra}}^{\text{img}}$ denote content and degradation embeddings respectively. Prior works such as DA-CLIP [50] rely on symmetric InfoNCE objectives [61] for both content and degradation losses to enforce strict one-to-one alignment between images and degradation captions. However, mixed degradations often

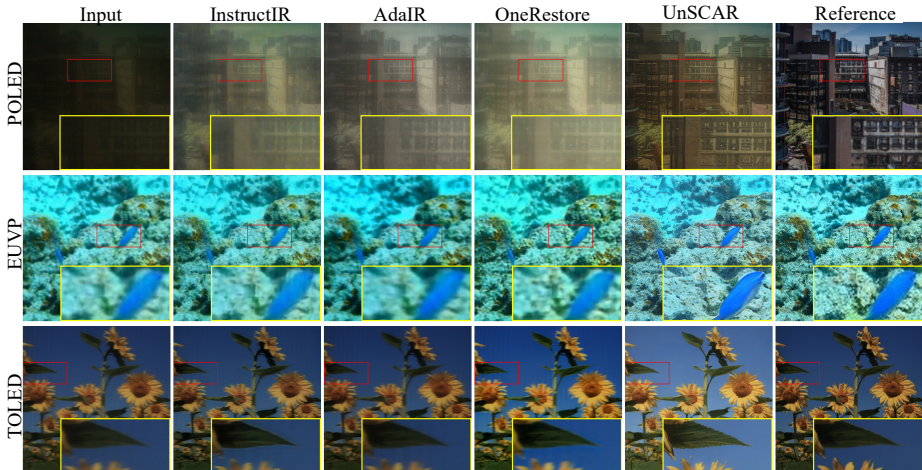


Fig. 6: *Generalization to unseen degradations.* Zero-shot evaluation of baseline methods and our approach on unseen mixed-degradation datasets.

share similarities across multiple categories, making hard contrastive pairing suboptimal. We adopt the **sigmoid loss** from SigLIP [82] for $\mathcal{L}_{\text{degradation}}$, which independently scores each image-caption pair via sigmoid activation (see Fig. 4).

Expert Routers Stabilization Strategy. To prevent expert routers from converging to suboptimal local minima or collapsing into a premature “winner-takes-all” regime, we employ a two-stage curriculum training strategy with label smoothing. Instead of using hard routing targets, we introduce controlled entropy into the routing distribution. During the initial exploration phase, we assign $\alpha \approx 0.8$ probability mass uniformly across task-relevant experts and distribute the remaining $(1 - \alpha)$ mass among suboptimal experts. This higher-entropy target maintains gradient flow across routing paths, mitigating dead-expert collapse and encouraging robust specialization. In the fine-tuning phase, the target mass for optimal experts is increased to 0.95, reducing entropy and promoting sparse, confident routing decisions. This curriculum progressively transitions the router from exploratory soft assignment to stable, task-discriminative expert selection. *Additional implementation details are provided in the supplementary material.*

4 Experiments and Results

4.1 Dataset and Metrics

We collect and curate a large-scale paired degradation dataset comprising 16 single-degradation, 10 mixed-degradation, and 3 real-world degradation (used only for evaluation) datasets. Detailed dataset composition is provided in the supplementary. Training data predominantly consist of natural outdoor images exhibiting real-world degradations, paired with clean targets. To evaluate performance under mixed degradations, we additionally curate synthetic combinations including (low light, rain, haze) from CDD [26], (low light, blur, noise) from LOL-Blur [94], and (low resolution, low light) from RELISUR [1]. All methods are evaluated using pixel-wise (i.e. PSNR, SSIM) and perceptual metrics

Table 2: Single-degradation restoration performance. All models are trained jointly on all tasks to evaluate scalability. **Bold** denotes best performance; underline indicates second best. ■ and ■ denotes prior single-task and all-in-one restoration models.

Method		<i>Dehazing</i> : RESIDE [38]			<i>Motion Deblur</i> : RHM [84]			<i>Low-Light</i> : LOL [74]			<i>Denoising</i> : CBSD68 [52]		
		PSNR ↑	SSIM ↑	LPIPS ↓	PSNR ↑	SSIM ↑	LPIPS ↓	PSNR ↑	SSIM ↑	LPIPS ↓	PSNR ↑	SSIM ↑	LPIPS ↓
■	Restormer [80]	26.57	0.95	0.05	26.41	0.81	0.35	20.43	0.83	0.30	28.60	0.79	0.23
	NAFNet [12]	27.62	0.96	0.04	27.87	0.84	0.24	22.19	0.88	0.16	32.71	0.89	0.08
	PromptIR [59]	26.27	0.95	0.03	<u>28.69</u>	<u>0.86</u>	<u>0.18</u>	18.58	0.83	0.20	30.52	0.84	0.16
■	OneRestore [26]	<u>30.68</u>	<u>0.97</u>	0.02	27.95	0.82	0.27	22.21	0.88	0.19	<u>32.27</u>	<u>0.88</u>	0.11
	InstructIR [14]	29.78	<u>0.97</u>	0.02	27.14	0.83	0.24	<u>22.33</u>	<u>0.89</u>	<u>0.14</u>	32.10	<u>0.88</u>	0.10
	AdaIR [16]	24.71	0.92	0.07	26.34	0.79	0.30	17.26	0.82	0.33	25.43	0.76	0.27
	AwRaCle [63]	25.65	0.93	0.07	25.27	0.80	0.26	17.95	0.80	0.31	26.79	0.77	0.27
UNSCAR		31.89	0.98	0.03	29.44	0.92	0.16	22.51	0.93	0.12	31.85	<u>0.88</u>	<u>0.09</u>
Method		<i>Defocus Deblur</i> : LSD [84]			<i>Desnowing</i> : SRRS [10]			<i>Deraining</i> : Rain4K [11]			<i>DeRaindrop</i> : Raindrop [32]		
		PSNR ↑	SSIM ↑	LPIPS ↓	PSNR ↑	SSIM ↑	LPIPS ↓	PSNR ↑	SSIM ↑	LPIPS ↓	PSNR ↑	SSIM ↑	LPIPS ↓
■	Restormer [80]	22.35	0.80	0.56	28.52	0.92	0.09	26.85	0.84	0.23	20.57	0.58	0.53
	NAFNet [12]	22.61	<u>0.83</u>	<u>0.35</u>	28.84	0.93	0.07	<u>28.38</u>	<u>0.89</u>	0.16	<u>23.75</u>	<u>0.71</u>	<u>0.35</u>
	PromptIR [59]	22.30	0.74	0.40	29.15	<u>0.94</u>	<u>0.06</u>	29.80	0.92	0.08	21.97	0.62	0.44
■	OneRestore [26]	22.75	0.75	0.43	28.98	0.93	0.08	26.51	0.84	0.16	22.43	0.65	0.45
	InstructIR [14]	<u>23.52</u>	0.76	0.39	29.04	<u>0.94</u>	0.07	25.22	0.84	0.16	22.33	0.65	0.46
	AdaIR [16]	20.09	0.68	0.56	28.44	0.92	0.08	23.85	0.74	0.26	18.87	0.50	0.53
	AwRaCle [63]	20.60	0.70	0.55	<u>29.22</u>	<u>0.94</u>	<u>0.06</u>	25.06	0.78	0.23	19.07	0.53	0.56
UNSCAR		23.62	0.84	0.25	31.39	0.97	0.03	29.30	0.91	0.09	24.03	0.72	0.31
Method		<i>Overexposure</i> : EED [2]			<i>Total Dark</i> : Sony TDD [78]			<i>JPEG</i> : Flickr2K [3]			<i>Superresolution</i> : RealSR [8]		
		PSNR ↑	SSIM ↑	LPIPS ↓	PSNR ↑	SSIM ↑	LPIPS ↓	PSNR ↑	SSIM ↑	LPIPS ↓	PSNR ↑	SSIM ↑	LPIPS ↓
■	Restormer [80]	20.75	0.88	0.15	19.02	0.64	0.62	27.43	0.88	0.12	32.77	0.92	0.13
	NAFNet [12]	21.32	0.91	<u>0.10</u>	20.88	0.69	<u>0.53</u>	28.93	0.89	0.13	38.70	0.96	0.06
	PromptIR [59]	17.62	0.87	0.15	20.43	0.62	0.58	29.34	0.90	0.12	36.01	<u>0.94</u>	<u>0.09</u>
■	OneRestore [26]	20.90	0.92	<u>0.10</u>	<u>21.46</u>	<u>0.71</u>	0.57	29.61	0.90	0.12	34.11	0.93	<u>0.09</u>
	InstructIR [14]	<u>21.57</u>	<u>0.92</u>	<u>0.10</u>	20.29	0.69	0.55	<u>29.65</u>	<u>0.91</u>	<u>0.10</u>	36.73	0.93	<u>0.09</u>
	AdaIR [16]	19.77	0.90	0.14	18.84	0.61	0.65	27.09	0.88	0.13	31.98	0.92	0.13
	AwRaCle [63]	17.65	0.86	0.17	19.47	0.55	0.64	27.68	0.88	0.14	31.35	0.92	0.14
UNSCAR		22.55	0.96	0.08	21.92	0.74	0.37	30.84	0.95	0.07	37.36	0.94	0.07
(Generative Tasks)		<i>Inpainting</i> : CelebA [48]			<i>Old Photo</i> : MLRN [27]			<i>Gray2Color</i> : Div2K [4]			<i>Deshadowing</i> : SRD [25]		
Method		PSNR ↑	SSIM ↑	LPIPS ↓	PSNR ↑	SSIM ↑	LPIPS ↓	PSNR ↑	SSIM ↑	LPIPS ↓	PSNR ↑	SSIM ↑	LPIPS ↓
■	Restormer [80]	22.03	0.85	0.28	18.37	0.84	0.35	21.70	0.92	0.21	18.71	0.82	0.18
	NAFNet [12]	26.64	0.89	0.15	27.08	0.92	0.16	27.97	0.93	0.13	28.96	<u>0.90</u>	<u>0.09</u>
	PromptIR [59]	23.25	0.88	0.21	21.35	0.89	0.22	25.80	0.94	0.14	22.51	0.86	0.14
■	OneRestore [26]	27.01	<u>0.91</u>	0.16	27.11	0.94	0.17	27.63	0.94	0.14	29.64	0.89	0.10
	InstructIR [14]	<u>27.12</u>	<u>0.91</u>	<u>0.15</u>	29.06	0.96	0.11	29.68	0.98	0.07	29.61	<u>0.90</u>	0.10
	AdaIR [16]	18.04	0.78	0.39	17.81	0.83	0.36	22.05	0.85	0.21	16.98	0.80	0.19
	AwRaCle [63]	22.99	0.88	0.24	19.80	0.84	0.32	24.51	0.89	0.16	21.30	0.85	0.17
UNSCAR		27.78	0.97	0.08	28.70	0.93	0.13	28.15	0.96	0.09	31.32	0.95	0.05

(LPIPS [87], DISTs [18]). We further report non-reference IQA metrics (NIQE [56], BRISQUE [55]) to evaluate on completely unseen degradations.

4.2 SOTA comparison on Single-Degradation Removal

We first compare UNSCAR with prior universal restoration models [26, 59, 63] on single-degradation restoration benchmarks [10, 11, 38, 52, 74]. For fair comparison, all competing models are trained on the same unified training corpus as UNSCAR. Results in Tab. 2 show that UNSCAR achieves state-of-the-art performance on 11 out of 16 benchmarks across all metrics, while remaining highly competitive on the others. These results highlight the strong scalability of UNSCAR across diverse restoration tasks, where prior methods often become suboptimal when trained jointly on multiple degradations. Qualitative comparisons in Fig. 5 further demonstrate that UNSCAR restores fine details more faithfully across tasks, including tiny objects (defocus and motion deblurring), distinct hair strands (face inpainting), and intricate building structures (raindrop removal). Overall, these results establish UNSCAR as a new state-of-the-art universal restoration model with strong generalization across diverse degradation types.

4.3 Unseen, Mixed-degradation and In-the-Wild Restoration

We evaluate UNSCAR on seen and unseen mixed-degradation datasets in a zero-shot setting (Tab. 3). UNSCAR consistently outperforms prior approaches



Fig. 7: Mixed restoration. Zero-shot evaluation of baseline methods vs ours for mixed restoration dataset with individual tasks seen during training.



Fig. 8: In-the-wild degradation removal. Comparison with the diffusion based DA-CLIP method on heavy indoor smoke removal [88].

by significant margins on both reference and no-reference metrics. Qualitative results (Figs. 6 and 7) confirm superior restoration of fine structures and de-blurred scenes, particularly on severely degraded cases such as low-light POLED and lowlight+blur images. On the in-the-wild dehazing dataset REVIDE [88], UNSCAR outperforms DA-CLIP [50] on PSNR and LPIPS while remaining competitive on SSIM (Tab. 6 and Fig. 8), demonstrating strong generalization to compound degradations across both in-domain and out-of-domain scenarios.

4.4 Additional Experiments

OOD and Few-shot Task Adaptation: Taking a step further, we extend UNSCAR to completely out-of-distribution tasks – medical image restoration. Specifically, we test on Laparoscopic De-smoking [76] and Fundus Image Restoration [67]. As described in Sec. 4.4, we employed our PEFT method to fine-tune UNSCAR on these benchmarks, and compared against a recent SOTA method BioIR [15] in Tab. 4, with qualitative samples in Fig. 10. UNSCAR shows highly competitive performance against the specialist in-domain BioIR (single₁- and multi₂-task) across all metrics ($\Delta_{PSNR} \approx 2.0 \downarrow$, $\Delta_{SSIM} \approx 0.02 \uparrow$, $\Delta_{DISTS} \approx 0.01 \downarrow$), showing robust generalization to OOD settings. Additionally, we also tested few-shot adaptability on two additional tasks – Demoiring [79]

Table 3: Zero-shot performance on unseen-mixed (left) and mixed datasets (right). The best performing models across all tasks from Table 1 were used for evaluations.

Method	TOLED [95]		POLED [95]		EUVP [30]		Haze+Snow [26]		Low-Blur [94]	
	NIQE↓	BRISQUE↓	NIQE↓	BRISQUE↓	NIQE↓	BRISQUE↓	PSNR↑	LPIPS↓	PSNR↑	LPIPS↓
Restormer [80]	6.95	46.69	10.38	27.58	7.30	57.93	17.68	0.222	13.92	0.381
NAFNet [12]	6.90	49.58	6.65	34.42	6.76	50.37	17.40	0.186	16.45	0.312
OneRestore [26]	6.93	52.97	6.49	16.57	7.43	56.45	17.00	0.210	12.84	0.402
InstructIR [14]	7.16	49.05	7.06	35.08	6.83	50.89	16.91	0.219	15.31	0.334
AdaIR [16]	7.07	44.99	6.96	25.06	7.40	54.60	17.70	0.261	14.15	0.375
Prompt-IR [59]	5.67	36.86	8.42	23.42	6.58	43.83	16.78	0.21	10.94	0.431
AwRaCle [63]	5.61	34.77	8.59	15.56	7.36	52.31	16.47	0.26	17.22	0.328
UnSCAR	3.97	25.13	5.21	16.21	3.58	20.77	21.96	0.12	20.59	0.255



Fig. 9: *Fewshot generalization.* One ($K=1$) to Few ($K \leq 50$) shot generalization performance over demoiréing and demosaicing tasks.

Table 4: *OOD Adaptation.* Generalization to unseen medical image restoration.

Method	Fundus IR [67]			Laparoscopic IR [76]		
	PSNR \uparrow	SSIM \uparrow	DISTS \downarrow	PSNR \uparrow	SSIM \uparrow	DISTS \downarrow
BioIR $_1$ [15]	31.94	0.96	0.09	28.55	0.90	0.07
BioIR $_2$ [15]	31.23	0.93	0.08	27.10	0.82	0.06
UnSCAR	29.60	0.95	0.09	27.81	0.95	0.05

Table 5: *Few-shot Adaptation* to unseen tasks: Demoiréing and Demosaicing.

Support Set	Demoiréing [79]			Demosaicing [64]		
	PSNR \uparrow	SSIM \uparrow	LPIPS \downarrow	PSNR \uparrow	SSIM \uparrow	LPIPS \downarrow
$K = 1$	20.67	0.76	0.24	20.09	0.77	0.291
$K = 5$	21.85	0.82	0.18	22.09	0.83	0.213
$K = 20$	22.37	0.84	0.17	22.18	0.84	0.210
$K = 50$	22.58	0.89	0.15	22.33	0.89	0.181

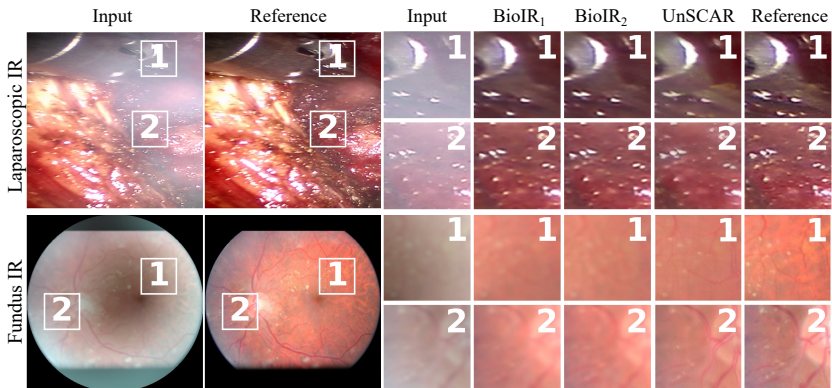


Fig. 10: *Medical.* Our model adapts to out-of-distribution data such as medical images.

and Demosaicing [64] – where we varied the few-shot support set size, tabulated in Tab. 5 (visual samples in Fig. 9). UNSCAR improves with increased support samples as well as show reliable performance even under low-data regimes.

Test-time Controllability via Sliders: Lastly, we examine UNSCAR’s test-time slider control (described previously in Sec. 4.4), showing qualitative results in Fig. 11. the α values denote the respective weights given to the degradations present. We can see that the model faithfully follows the weight assigned to each degradation i.e. if dehazing is higher it prioritizes haze removal, and so on. This asserts the reliability of our control sliders during test-time for UNSCAR.

4.5 Ablation Study

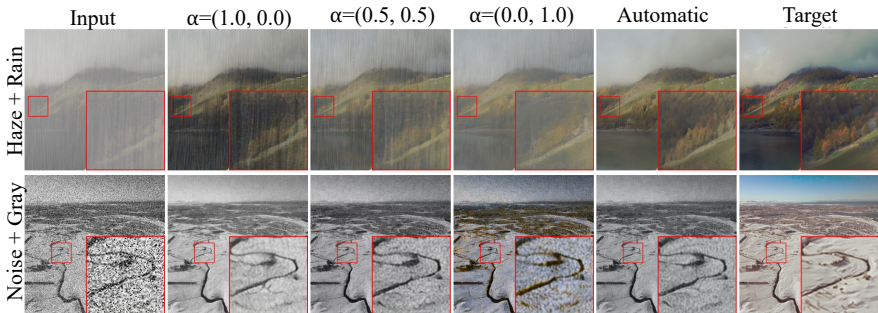
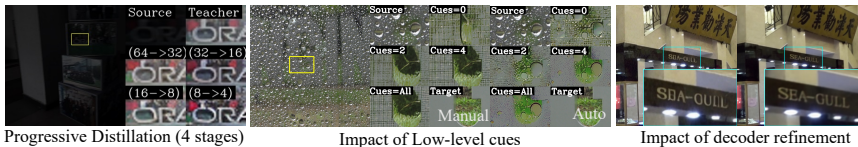
We perform ablations on our model to test restoration quality with respect to minimum number of sampling steps required for inference, impact of low level cues (v_i), control signal strength (default is 1.0) and impact of decoder finetuning as shown in Fig. 12 and Tab. 7. We perform progressive distillation [53] of our frozen diffusion backbone (keeping restoration control module frozen) to reduce sampling to 4 steps ($\sim 10x$) without loss of quality. Loss of low-level cues impact the quality of restoration heavily during automatic restoration when no user prior

Table 6: *In-the-wild* performance against DA-CLIP [50] variants.

Method	Real-Fog [88]		
	PSNR \uparrow	SSIM \uparrow	LPIPS \downarrow
DACLIP _{UIR}	14.23	0.751	0.428
DACLIP _{mix}	15.44	0.66	0.433
DACLIP _W	14.18	0.61	0.471
UNSCAR	16.07	0.72	0.353

Table 7: *Ablation studies.* Impact of sampling steps, low-level cues, and control signal strength.

%age	Sampling Steps		Low-level cues		Control Strength	
	PSNR \uparrow	LPIPS \downarrow	PSNR \uparrow	LPIPS \downarrow	PSNR \uparrow	LPIPS \downarrow
% = 1.0	28.29	0.126	28.29	0.126	28.29	0.126
% = 0.5	28.48	0.131	28.20	0.131	24.52	0.254
% = 0.2	27.80	0.132	27.61	0.136	19.84	0.438
% = 0.1	27.88	0.144	26.96	0.144	16.21	0.615

**Fig. 11:** *Controllability.* Our model supports slider-based control of the level of restoration per degradation. α denotes the aberration strength (haze vs. rain, noise vs. gray).**Fig. 12:** *Ablation studies.* We analyze model performance under reduced sampling steps (left) and fewer low-level cues under automatic versus user controlled restoration (middle), and the impact of decoder refinement on structural preservation (right).

knowledge is available about existing degradations. Decoder finetuning helps preserve structural details such as text lost during the diffusion process.

5 Conclusion

We presented UNSCAR, a universal image restoration framework designed to scale across diverse and simultaneous degradation types while enabling controllable and adaptable restoration. Our method combines degradation-aware representations with a mixture-of-experts generative backbone, mitigating cross-degradation interference and supporting stable learning across a large set of degradations. In addition, we proposed degradation control sliders as a simple yet effective mechanism for user-driven restoration. We also introduced a lightweight parameter-efficient adaptation strategy, enabling efficient transfer to unseen domains. Extensive experiments across single, mixed, and out-of-distribution restoration benchmarks demonstrate the superiority, robustness and flexibility of the proposed approach. UNSCAR represents a step toward practical, general-purpose restoration systems capable of operating reliably under diverse real-world conditions. We hope this work motivates future research toward scalable and controllable frameworks for universal image restoration.

References

1. Aakerberg, A., Nasrollahi, K., Moeslund, T.B.: Rellisur: A real low-light image super-resolution dataset. In: Thirty-fifth Conference on Neural Information Processing Systems Datasets and Benchmarks Track (Round 2) (2021) **10**
2. Affi, M., Derpanis, K.G., Ommer, B., Brown, M.S.: Learning multi-scale photo exposure correction. In: Proceedings of the IEEE Conference on Computer Vision and Pattern Recognition (2021) **11**
3. Agustsson, E., Timofte, R.: Ntire 2017 challenge on single image super-resolution: Dataset and study. In: The IEEE Conference on Computer Vision and Pattern Recognition (CVPR) Workshops (July 2017) **11**
4. Agustsson, E., Timofte, R.: Ntire 2017 challenge on single image super-resolution: Dataset and study. In: CVPR Workshops (2017) **11**
5. Ai, Y., Huang, H., Zhou, X., Wang, J., He, R.: Multimodal prompt perceiver: Empower adaptiveness generalizability and fidelity for all-in-one image restoration. In: Proceedings of the IEEE/CVF Conference on Computer Vision and Pattern Recognition. pp. 25432–25444 (2024) **2, 4**
6. Akhatova, V., Nosirova, D., Zakiryayeva, P., Normamatov, B., Kuvandikov, G., Meqdad, M.N., Zearah, S.A., et al.: Stable diffusion model for image restoration to enhance low-quality satellite images. In: 2025 3rd International Conference on Cyber Resilience (ICCR). pp. 1–7. IEEE (2025) **2**
7. Blattmann, A., Rombach, R., Ling, H., Dockhorn, T., Kim, S.W., Fidler, S., Kreis, K.: Align your latents: High-resolution video synthesis with latent diffusion models. In: CVPR (2023) **3**
8. Cai, J., Zeng, H., Yong, H., Cao, Z., Zhang, L.: Toward real-world single image super-resolution: A new benchmark and a new model. In: Proceedings of the IEEE/CVF international conference on computer vision. pp. 3086–3095 (2019) **11**
9. Chen, H., Wang, Y., Guo, T., Xu, C., Deng, Y., Liu, Z., Ma, S., Xu, C., Xu, C., Gao, W.: Pre-trained image processing transformer. In: CVPR (2021) **3**
10. Chen, H., Ren, J., Gu, J., Wu, H., Lu, X., Cai, H., Zhu, L.: Snow removal in video: A new dataset and a novel method. In: 2023 IEEE/CVF International Conference on Computer Vision (ICCV). pp. 13165–13176. iee (2023) **11**
11. Chen, H., Chen, X., Wu, C., Zheng, Z., Pan, J., Fu, X.: Towards ultra-high-definition image deraining: A benchmark and an efficient method. IEEE Transactions on Multimedia (2026) **11**
12. Chen, L., Chu, X., Zhang, X., Sun, J.: Simple baselines for image restoration. In: ECCV (2022) **1, 2, 5, 11, 12**
13. Cho, S.J., Ji, S.W., Hong, J.P., Jung, S.W., Ko, S.J.: Rethinking coarse-to-fine approach in single image deblurring. In: ICCV (2021) **3**
14. Conde, M.V., Geigle, G., Timofte, R.: InstructIR: High-quality image restoration following human instructions. In: European Conference on Computer Vision. pp. 1–21. Springer (2024) **11, 12**
15. Cui, Y., Ren, W., Knoll, A.: Bio-inspired image restoration. In: The Thirty-ninth Annual Conference on Neural Information Processing Systems (2025) **12, 13**
16. Cui, Y., Zamir, S.W., Khan, S., Knoll, A., Shah, M., Khan, F.S.: AdaIR: Adaptive all-in-one image restoration via frequency mining and modulation. In: 13th international conference on learning representations, ICLR 2025. pp. 57335–57356. International Conference on Learning Representations, ICLR (2025) **11, 12**
17. Deng, J., Wu, X., Yang, Y., Zhu, C., Wang, S., Wu, Z.: Acquire and then adapt: Squeezing out text-to-image model for image restoration. In: Proceedings of the Computer Vision and Pattern Recognition Conference. pp. 23195–23206 (2025) **2**

18. Ding, K., Ma, K., Wang, S., Simoncelli, E.P.: Image quality assessment: Unifying structure and texture similarity. *IEEE transactions on pattern analysis and machine intelligence* **44**(5), 2567–2581 (2020) [11](#)
19. Dong, W., Zhou, H., Wang, R., Liu, X., Zhai, G., Chen, J.: Dehazedct: Towards effective non-homogeneous dehazing via deformable convolutional transformer. In: *CVPR Workshops* (2024) [1](#), [3](#)
20. Fan, L., Zhang, F., Fan, H., Zhang, C.: Brief review of image denoising techniques. *Visual Computing for Industry, Biomedicine, and Art* (2019) [3](#)
21. Gandelsman, Y., Shocher, A., Irani, M.: "double-dip": unsupervised image decomposition via coupled deep-image-priors. In: *CVPR* (2019) [1](#), [2](#), [3](#)
22. Gandikota, R., Materzyńska, J., Zhou, T., Torralba, A., Bau, D.: Concept sliders: Lora adaptors for precise control in diffusion models. In: *European Conference on Computer Vision*. pp. 172–188. Springer (2024) [2](#), [4](#)
23. Gandikota, R., Orgad, H., Belinkov, Y., Materzyńska, J., Bau, D.: Unified concept editing in diffusion models. In: *Proceedings of the IEEE/CVF Winter Conference on Applications of Computer Vision*. pp. 5111–5120 (2024) [2](#), [4](#)
24. Gao, H., Yang, J., Zhang, Y., Wang, N., Yang, J., Dang, D.: Prompt-based ingredient-oriented all-in-one image restoration. *IEEE Transactions on Circuits and Systems for Video Technology* **34**(10), 9458–9471 (2024) [2](#)
25. Guo, L., Wang, C., Wang, Y., Huang, S., Yang, W., Kot, A.C., Wen, B.: Single-image shadow removal using deep learning: A comprehensive survey. *arXiv preprint arXiv:2407.08865* (2024) [11](#)
26. Guo, Y., Gao, Y., Lu, Y., Zhu, H., Liu, R.W., He, S.: Onerestore: A universal restoration framework for composite degradation. *arXiv preprint arXiv:2407.04621* (2024) [1](#), [2](#), [10](#), [11](#), [12](#)
27. Hao, Q.: MLRN (2023). <https://doi.org/10.17632/r4zm9sj6cf.1>, <https://doi.org/11>
28. He, C., Shen, Y., Fang, C., Xiao, F., Tang, L., Zhang, Y., Zuo, W., Guo, Z., Li, X.: Diffusion models in low-level vision: A survey. *arXiv preprint arXiv:2406.11138* (2024) [4](#)
29. Ho, J., Jain, A., Abbeel, P.: Denoising diffusion probabilistic models. *NeurIPS* (2020) [3](#)
30. Islam, M.J., Xia, Y., Sattar, J.: Fast underwater image enhancement for improved visual perception. *IEEE robotics and automation letters* **5**(2), 3227–3234 (2020) [12](#)
31. Jiang, Y., Zhang, Z., Xue, T., Gu, J.: Autodir: Automatic all-in-one image restoration with latent diffusion. *arXiv preprint arXiv:2310.10123* (2023) [1](#), [2](#), [3](#), [4](#)
32. Jin, Y., Li, X., Wang, J., Zhang, Y., Zhang, M.: Raindrop clarity: A dual-focused dataset for day and night raindrop removal. In: *European Conference on Computer Vision*. pp. 1–17. Springer (2024) [11](#)
33. Karras, T., Laine, S., Aittala, M., Hellsten, J., Lehtinen, J., Aila, T.: Analyzing and improving the image quality of stylegan. In: *CVPR* (2020) [7](#)
34. Kawar, B., Elad, M., Ermon, S., Song, J.: Denoising diffusion restoration models. *NeurIPS* (2022) [3](#)
35. Kemker, R., McClure, M., Abitino, A., Hayes, T., Kanan, C.: Measuring catastrophic forgetting in neural networks. In: *AAAI* (2018) [2](#)
36. Labs, B.F.: Flux. <https://github.com/black-forest-labs/flux> (2024) [2](#), [3](#)
37. Lehtinen, J.: Noise2noise: Learning image restoration without clean data. *arXiv preprint arXiv:1803.04189* (2018) [3](#)
38. Li, B., Ren, W., Fu, D., Tao, D., Feng, D., Zeng, W., Wang, Z.: Benchmarking single-image dehazing and beyond. *IEEE TIP* (2019) [11](#)
39. Li, B., Gou, Y., Gu, S., Liu, J.Z., Zhou, J.T., Peng, X.: You only look yourself: Unsupervised and untrained single image dehazing neural network. *IJCV* (2021) [3](#)

40. Li, B., Gou, Y., Liu, J.Z., Zhu, H., Zhou, J.T., Peng, X.: Zero-shot image dehazing. *IEEE TIP* (2020) **3**
41. Li, B., Liu, X., Hu, P., Wu, Z., Lv, J., Peng, X.: All-in-one image restoration for unknown corruption. In: *CVPR* (2022) **3**
42. Li, M., Yang, T., Kuang, H., Wu, J., Wang, Z., Xiao, X., Chen, C.: Controlnet++: Improving conditional controls with efficient consistency feedback: Project page: [liming-ai.github.io/controlnet_plus_plus](https://github.com/liming-ai/controlnet_plus_plus). In: *European Conference on Computer Vision*. pp. 129–147. Springer (2024) **3**
43. Li, R., Tan, R.T., Cheong, L.F.: All in one bad weather removal using architectural search. In: *CVPR* (2020) **3**
44. Li, W., Zhang, X., Chen, B., Xie, J., Wang, Y., Zhang, K., Li, J., Zhang, L., Zhang, J., Zhao, S.: Uare: A unified vision-language model for image quality assessment, restoration, and enhancement. *arXiv preprint arXiv:2512.06750* (2025) **2, 3, 4**
45. Li, X., Ren, Y., Jin, X., Lan, C., Wang, X., Zeng, W., Wang, X., Chen, Z.: Diffusion models for image restoration and enhancement: A comprehensive survey. *International Journal of Computer Vision* **133**(11), 8078–8108 (2025) **1, 4**
46. Li, Z., Lei, Y., Ma, C., Zhang, J., Shan, H.: Prompt-in-prompt learning for universal image restoration. *arXiv preprint arXiv:2312.05038* (2023) **3**
47. Liang, J., Cao, J., Sun, G., Zhang, K., Van Gool, L., Timofte, R.: Swinir: Image restoration using swin transformer. In: *ICCV Workshops* (2021) **3**
48. Liu, Z., Luo, P., Wang, X., Tang, X.: Deep learning face attributes in the wild. In: *Proceedings of International Conference on Computer Vision (ICCV)* (December 2015) **11**
49. Luo, W., Qin, H., Chen, Z., Wang, L., Zheng, D., Li, Y., Liu, Y., Li, B., Hu, W.: Visual-instructed degradation diffusion for all-in-one image restoration. In: *Proceedings of the Computer Vision and Pattern Recognition Conference* (2025) **1, 2**
50. Luo, Z., Gustafsson, F.K., Zhao, Z., Sjölund, J., Schön, T.B.: Controlling vision-language models for multi-task image restoration. *arXiv preprint arXiv:2310.01018* (2023) **1, 2, 3, 4, 6, 9, 12, 14**
51. Mandal, D., Chattopadhyay, S., Tong, G., Chakravarthula, P.: Unicorn: Latent diffusion-based unified controllable image restoration network across multiple degradations. In: *WACV* (2026) **1, 2, 3, 4, 6, 7**
52. Martin, D., Fowlkes, C., Tal, D., Malik, J.: A database of human segmented natural images and its application to evaluating segmentation algorithms and measuring ecological statistics. In: *ICCV* (2001) **11**
53. Meng, C., Rombach, R., Gao, R., Kingma, D., Ermon, S., Ho, J., Salimans, T.: On distillation of guided diffusion models. In: *Proceedings of the IEEE/CVF conference on computer vision and pattern recognition*. pp. 14297–14306 (2023) **13**
54. Midjourney, Inc.: Midjourney (2024), <https://www.midjourney.com>, version 6 **2**
55. Mittal, A., Moorthy, A.K., Bovik, A.C.: No-reference image quality assessment in the spatial domain. *IEEE TIP* (2012) **11**
56. Mittal, A., Soundararajan, R., Bovik, A.C.: Making a “completely blind” image quality analyzer. *IEEE SPL* (2012) **11**
57. Peng, B., Wang, J., Zhang, Y., Li, W., Yang, M.C., Jia, J.: Controlnext: Powerful and efficient control for image and video generation. *arXiv preprint arXiv:2408.06070* (2024) **3**
58. Poole, B., Jain, A., Barron, J.T., Mildenhall, B.: Dreamfusion: Text-to-3d using 2d diffusion. In: *ICLR* (2023) **3**
59. Potlapalli, V., Zamir, S.W., Khan, S.H., Shahbaz Khan, F.: PromptIR: Prompting for all-in-one image restoration. *NeurIPS* (2024) **1, 2, 3, 11, 12**

60. Radford, A., Kim, J.W., Hallacy, C., Ramesh, A., Goh, G., Agarwal, S., Sastry, G., Askell, A., Mishkin, P., Clark, J., et al.: Learning transferable visual models from natural language supervision. In: ICML (2021) **4**
61. Radford, A., Kim, J.W., Hallacy, C., Ramesh, A., Goh, G., Agarwal, S., Sastry, G., Askell, A., Mishkin, P., Clark, J., et al.: Learning transferable visual models from natural language supervision. In: International conference on machine learning. pp. 8748–8763. PmLR (2021) **6, 9**
62. Rajagopalan, S., Narayan, K., Patel, V.M.: Restorevar: Visual autoregressive generation for all-in-one image restoration. In: ICLR (2026) **1, 2, 3, 4**
63. Rajagopalan, S., Patel, V.M.: Awracle: All-weather image restoration using visual in-context learning. arXiv preprint arXiv:2409.00263 (2024) **1, 2, 11, 12**
64. Research, M.: Microsoft research cambridge demosaicing dataset (2015), <https://www.microsoft.com/en-us/download/details.aspx?id=52535>, accessed: [Insert Date Here] **13**
65. Rombach, R., Blattmann, A., Lorenz, D., Esser, P., Ommer, B.: High-resolution image synthesis with latent diffusion models. In: CVPR. pp. 10684–10695 (2022) **2, 3, 7**
66. Ruiz, N., Li, Y., Jampani, V., Pritch, Y., Rubinstein, M., Aberman, K.: Dreambooth: Fine tuning text-to-image diffusion models for subject-driven generation. In: CVPR (2023) **3**
67. Shen, Z., Fu, H., Shen, J., Shao, L.: Modeling and enhancing low-quality retinal fundus images. IEEE Transactions on Medical Imaging **40**(3), 996–1006 (2020) **2, 3, 12, 13**
68. Song, J., Meng, C., Ermon, S.: Denoising diffusion implicit models. arXiv preprint arXiv:2010.02502 (2020) **8**
69. Song, Y., He, Z., Qian, H., Du, X.: Vision transformers for single image dehazing. IEEE TIP (2023) **1, 3**
70. Valanarasu, J.M.J., Yasarla, R., Patel, V.M.: Transweather: Transformer-based restoration of images degraded by adverse weather conditions. In: CVPR (2022) **3**
71. Wan, T., Wang, A., Ai, B., Wen, B., Mao, C., Xie, C.W., Chen, D., Yu, F., Zhao, H., Yang, J., et al.: Wan: Open and advanced large-scale video generative models. arXiv preprint arXiv:2503.20314 (2025) **3**
72. Wang, P., Luo, X., Xie, Y., Qu, Y.: Data-free distillation with degradation-prompt diffusion for multi-weather image restoration. arXiv preprint arXiv:2409.03455 (2024) **4**
73. Wang, Z., Cun, X., Bao, J., Zhou, W., Liu, J., Li, H.: Uformer: A general u-shaped transformer for image restoration. In: CVPR (2022) **3**
74. Wei, C., Wang, W., Yang, W., Liu, J.: Deep retinex decomposition for low-light enhancement. arXiv preprint arXiv:1808.04560 (2018) **11**
75. Wu, C., Wang, P., Zheng, Z.: Re-examine all-in-one image restoration: A catastrophic forgetting perspective. Pattern Recognition Letters (2025) **2**
76. Xia, W., Peters, T.M., Fan, V., Sthanunathan, H., Qi, O., Chen, E.C.: In vivo laparoscopic image de-smoking dataset, evaluation, and beyond. IEEE Transactions on Medical Imaging (2025) **2, 3, 12, 13**
77. xinsir6: Controlnet++: All-in-one controlnet for image generations and editing! <https://github.com/xinsir6/ControlNetPlus> (2024), accessed: 2025 **7**
78. Yan, Q., Feng, Y., Zhang, C., Wang, P., Wu, P., Dong, W., Sun, J., Zhang, Y.: You only need one color space: An efficient network for low-light image enhancement. arXiv preprint arXiv:2402.05809 (2024) **11**
79. Yu, X., Dai, P., Li, W., Ma, L., Shen, J., Li, J., Qi, X.: Towards efficient and scale-robust ultra-high-definition image demoiréing. In: European Conference on Computer Vision. pp. 646–662. Springer (2022) **12, 13**

80. Zamir, S.W., Arora, A., Khan, S., Hayat, M., Khan, F.S., Yang, M.H.: Restormer: Efficient transformer for high-resolution image restoration. In: CVPR (2022) [1](#), [2](#), [3](#), [11](#), [12](#)
81. Zavadski, D., Feiden, J.F., Rother, C.: Controlnet-xs: Rethinking the control of text-to-image diffusion models as feedback-control systems. In: European Conference on Computer Vision. pp. 343–362. Springer (2024) [3](#), [7](#)
82. Zhai, X., Mustafa, B., Kolesnikov, A., Beyer, L.: Sigmoid loss for language image pre-training. In: Proceedings of the IEEE/CVF international conference on computer vision. pp. 11975–11986 (2023) [8](#), [10](#)
83. Zhang, K., Ren, W., Luo, W., Lai, W.S., Stenger, B., Yang, M.H., Li, H.: Deep image deblurring: A survey. IJCV (2022) [3](#)
84. Zhang, K., Wang, T., Luo, W., Chen, B., Ren, W., Stenger, B., Liu, W., Li, H., Ming-Hsuan, Y.: Mc-blur: A comprehensive benchmark for image deblurring. In: IEEE Transactions on Circuits and Systems for Video Technology (2023) [11](#)
85. Zhang, L., Rao, A., Agrawala, M.: Adding conditional control to text-to-image diffusion models. In: ICCV (2023) [3](#), [4](#)
86. Zhang, L., Rao, A., Agrawala, M.: Adding conditional control to text-to-image diffusion models. In: Proceedings of the IEEE/CVF international conference on computer vision. pp. 3836–3847 (2023) [3](#)
87. Zhang, R., Isola, P., Efros, A.A., Shechtman, E., Wang, O.: The unreasonable effectiveness of deep features as a perceptual metric. In: CVPR (2018) [11](#)
88. Zhang, X., Dong, H., Pan, J., Zhu, C., Tai, Y., Wang, C., Li, J., Huang, F., Wang, F.: Learning to restore hazy video: A new real-world dataset and a new method. In: CVPR. pp. 9239–9248 (2021) [12](#), [14](#)
89. Zhao, C., Guo, P., Yang, D., Tang, Y., He, Y., Simon, B., Belue, M., Harmon, S., Turkbey, B., Xu, D.: Maisi-v2: Accelerated 3d high-resolution medical image synthesis with rectified flow and region-specific contrastive loss. arXiv preprint arXiv:2508.05772 (2025) [3](#)
90. Zhao, S., Chen, D., Chen, Y.C., Bao, J., Hao, S., Yuan, L., Wong, K.Y.K.: Uni-controlnet: All-in-one control to text-to-image diffusion models. Advances in Neural Information Processing Systems **36**, 11127–11150 (2023) [3](#)
91. Zhao, S., Chen, D., Chen, Y.C., Bao, J., Hao, S., Yuan, L., Wong, K.Y.K.: Uni-controlnet: All-in-one control to text-to-image diffusion models. In: NeurIPS (2024) [3](#)
92. Zheng, D., Wu, X.M., Yang, S., Zhang, J., Hu, J.F., Zheng, W.S.: Selective hourglass mapping for universal image restoration based on diffusion model. In: CVPR (2024) [4](#)
93. Zhou, M., Ye, K., Delbraccio, M., Milanfar, P., Patel, V.M., Talebi, H.: Unires: Universal image restoration for complex degradations. arXiv preprint arXiv:2506.05599 (2025) [2](#), [3](#), [4](#), [6](#)
94. Zhou, S., Li, C., Change Loy, C.: Lednet: Joint low-light enhancement and deblurring in the dark. In: ECCV (2022) [10](#), [12](#)
95. Zhou, Y., Ren, D., Emerton, N., Lim, S., Large, T.: Image restoration for under-display camera. In: Proceedings of the IEEE/CVF conference on computer vision and pattern recognition. pp. 9179–9188 (2021) [12](#)